Bootstrap Current Simulations with Experimental LHD Plasma Density and Temperature Profiles, Energy Scattering and Finite Orbit Width

Maxim Yu. ISAEV, Kiyomasa Y. WATANABE[1)], Shinsuke SATAKE[1)], Yuji NAKAMURA[2)] and Wilfred A. COOPER[3)]

National Research Centre "Kurchatov Institute", Moscow, 123182, Russia
[1)]*National Institute for Fusion Science, Toki 509-5292, Japan*
[2)]*Graduate School of Energy Science, Kyoto University, Uji 611-0011, Japan*
[3)]*Ecole Polytechnique Fédérale de Lausanne (EPFL), Centre de Recherches en Physique des Plasmas, Association Euratom-Confédération Suisse, CH-1015 Lausanne, Switzerland*

(Received 6 December 2011 / Accepted 26 April 2012)

Bootstrap current calculations with the neoclassical SPBSC and VENUS+δf codes have been performed on experimental Large Helical Device (LHD, NIFS, Japan) configurations with different magnetic axis positions and simplified plasma density and temperature profiles. In this paper, we use experimentally obtained electron density and temperature profiles for the LHD discharges #61863 and #82582 to compute the corresponding magnetohydrodynamic equilibrium states and collisional frequency. An improved collisional operator has been implemented into the VENUS+δf code. The comparison between the measured LHD bootstrap current and that expected from neoclassical simulations is discussed.

Keywords: heliotron, stellarator, magnetic configuration, neoclassical transport, bootstrap current, 3D numerical orbit, δf method

DOI: 10.1585/pfr.7.1403077

1. Introduction

The bootstrap current j_b is connected with collisional movements of the charged particles trapped in local mirror fields. For non-axisymmetric toroidal systems, the problems are connected with the complicated three-dimentional (3D) structure of the stellarator magnetic fields. Numerical tools to calculate the neoclassical bootstrap current in non-axisymmetric magnetic configurations use several models and approaches. The fast SPBSC code [1] based on a quasi-analytical fluid moment approach uses a monotonic approximation (connection formula) between the semi-analytical limits, including so-called long-mean-free-path (LMFP) or Shaing-Callen limit [2]. The SPBSC code has been successfully applied for the Large Helical Device (LHD, Japan) configurations [3] with different magnetic axis positions. A module [4] of the 3D ideal MHD TERPSICHORE code [5] computes the bootstrap current in the collisionless limit taking into account a wide spectrum of the magnetic field in Boozer coordinates [6] in addition to a resonance detuning procedure. These fast numerical tools based on semi-analytical limits provide the possibility to obtain iterative self-consistent equilibria with the bootstrap current and to compute the corresponding MHD stability [4].

Experimental verification of the validity of some of the earlier bootstrap current models in the ATF torsatron was examined in [7]. Validation of bootstrap current model in stellarator configurations has been performed for the Wendelstein-7AS (Germany) device [8] with the drift-kinetic equation solver (DKES) code [9]. In the long-mean-free-path regime, differences exist between the monoenergetic bootstrap current coefficients calculated with the DKES and SPBSC codes for several 3D configurations [10, 16], which motivates further development of new bootstrap current simulation tools.

Analysis of neoclassical transport in the banana regime with the DKES code for the LHD configuration with model magnetic field strength spectra and momentum conservation neglected has been presented in Ref. [11]. In that paper, the mono-energetic bootstrap current coefficient is analysed with respect to the collisionality as well as to the radial electric field. The results for finite but low collisionalities are compared with the collisionless limit [2]. The results show that the ion bootstrap current coefficients depend on the radial electric field.

The more time-consuming VENUS+δf code [12] uses guiding centre numerical orbits in Boozer coordinates calculated with the TERPSICHORE code, Monte Carlo pitch angle scattering [13] and a δf method to compute the neoclassical bootstrap current. A careful benchmark of the neoclassical coefficients for arbitrary collisionality

author's e-mail: isaev@nfi.kiae.ru

has been performed in the frame of the International Collaboration on Neoclassical Transport in Stellarators [14]. Good agreement of the monoenergetic bootstrap current coefficients with different radial electric field for various stellarator configurations (LHD, NCSX, W7X) was obtained with the DKES, VENUS+δf, NEO-MC and NEO-2 codes [15, 16]. Additional numerical efforts have been devoted with the VENUS+δf code to simulate the effect of different magnetic axis positions on the monoenergetic bootstrap current coefficients in LHD [17]. Total bootstrap current calculations with the updated VENUS+δf code that incorporates energy convolution and the momentum correction technique have been performed for the reference tokamak JT-60U cases and for the experimental LHD configurations with different magnetic axis positions, zero electric field and simplified plasma density and temperature profiles [18].

In this paper, we present the improved conservative collision operator [19] implemented in the VENUS+δf code with new correction terms which satisfy not only the momentum, but also energy and particle number conservation (Sec. 2). We use experimentally obtained plasma density and temperature profiles [20] to compute with the SPBSC, TERPSICHORE and VENUS+δf codes the corresponding magnetohydrodynamic equilibrium states and the neoclassical bootstrap current for the LHD discharge #61863 with the magnetic axis at $R_{\mathrm{axis}} = 3.90\,\mathrm{m}$ (Sec. 3) and for the LHD discharge #82582 with the magnetic axis at $R_{\mathrm{axis}} = 4.05\,\mathrm{m}$ (Sec. 4). These two LHD configurations with the different magnetic axes are selected for the simulations because the bootstrap current is significantly sensitive to the magnetic axis position. The measured LHD bootstrap current (with the help of motional Stark effect) is compared with that expected from neoclassical simulations.

2. Improved Conservative Collision Operator Implemented into the VENUS+δf Code

To calculate the neoclassical transport in heliotrons/stellarators, the VENUS+δf code uses accurate VENUS guiding centre numerical orbits [21] in 3D magnetic fields calculated with the TERPSICHORE code in Boozer coordinates. The equilibrium is computed with the ideal MHD VMEC2000 code [22] taking into account experimental plasma pressure profile and the complicated 3D shape of the plasma boundary magnetic surface of the experimental LHD configuration. The Coulomb collisions with the velocity dependent like-particle collisional frequency ν (V) are implemented in two steps. Pitch-angle and energy scattering is modelled by a standard Monte-Carlo procedure [13]. Then the perturbed distribution function $\delta f = w/p$ is modified to provide the particle number, energy and momentum conservation in a 2-weight evolution scheme [19, 23]:

$$\frac{\mathrm{d}w}{\mathrm{d}t} = -\frac{p}{f_{\mathrm{M}}} V_{\mathrm{d}} \nabla f_{\mathrm{M}} + pP_{\mathrm{S}}, \tag{1}$$

$$\frac{\mathrm{d}p}{\mathrm{d}t} = \frac{p}{f_{\mathrm{M}}} V_{\mathrm{d}} \nabla f_{\mathrm{M}}, \tag{2}$$

where V_{d} is the drift velocity of a particle with energy E and mass m, $f_{\mathrm{m}}(s, E) = n(s)(2\pi T(s)/m)^{-3/2} e^{-E/T(s)}$ is a local Maxwellian on the magnetic flux surface labelled as s, with plasma temperature $T(s) = m{V_{\mathrm{th}}}^2/2$ and density $n(s)$. s is proportional to the square of the normalized minor radius, $s = 1.0$ correspond to the plasma boundary. A full conservative collision operator is applied with the weight correction term

$$P_{\mathrm{S}} = -\delta N \left(1 - 3\sqrt{\frac{\pi}{2}}(\mu - \mu')/x\right) - \delta P \mu V_{\|} x^{-3} - \delta E(\mu - \mu')/x, \tag{3}$$

$$\mu(x) = erf(x) - (2/\sqrt{\pi}) x e^{-x^2}, \tag{4}$$

where $x = V/V_{\mathrm{th}}$, $V_{\|}$ is a particle velocity component parallel to the magnetic field with strength B. δN, δP, δE are the particle number, momentum and energy changes (errors) due to collisions, respectively, $\mu(x)$ is the Maxwellian integral. The ion bootstrap current density with a particle charge q and a phase-space volume element $\mathrm{d}\Omega$ is computed from time-averaging equation

$$\langle j_{\|} B \rangle = \left\langle \left(nq \sum V_{\|} B \delta f \mathrm{d}\Omega \right) \Big/ \left(\sum f_{\mathrm{M}} \mathrm{d}\Omega \right) \right\rangle \tag{5}$$

Our main assumption is the equal temperature and density profiles imposed on electrons and ions, which constitutes the current experimental LHD practice for these specific discharges. In this paper we consider two different methods to calculate the bootstrap current with the VENUS+δf code: (ii) using mainly the ions contribution and (ei) using the mixed electrons-ions contributions.

In the first method (ii) the radial electric field is neglected, the contribution of ions and electrons to the total bootstrap current is supposed to be equal; that simplifies the simulation process by limiting the computation to the ion fraction of the total current only (with ion-ion collisions). In the case of equal impact of ions and electrons, the flux derivative of the total current $\mathrm{d}J_{\mathrm{BS}}/\mathrm{d}s$ is obtained from equation

$$\mathrm{d}J_{\mathrm{BS}}/\mathrm{d}s = 2\pi a^2 \langle j_{\|} B \rangle / B_0, \tag{6}$$

where a is the average minor plasma radius and B_0 is the magnetic field strength on the magnetic axis, the total bootstrap current is

$$J_{\mathrm{BS}} = \int_0^1 \frac{\mathrm{d}J_{\mathrm{BS}}}{\mathrm{d}s} \mathrm{d}s \tag{7}$$

The second method (ei) to calculate the bootstrap current is described on pages 22-23 of the Ref. [16] together with the corresponding equations. The radial ambipolar

electric field is calculated from the zero ion radial flux condition ("ion root"), the ions contribution to the bootstrap current is small, the electrons contribution includes both electon-electron and electron-ion collisions and dominates in the bootstrap current.

In our previous paper [17] we used a one-weight evolution scheme with the momentum correction term $\Delta\delta f$ of the form, proposed in [24]:

$$\Delta\delta f = \frac{-\nu(V)V_{\|}\delta P f_{\mathrm{M}}}{\sum \nu V_{\|}^2 f_{\mathrm{M}} \mathrm{d}\Omega} \tag{8}$$

The difference between the application of the full conservative operator (3) and the application of the momentum correction term (8) is visible on the test JT-60 tokamak results [18] with the relative errors due to collisions and integration along the orbits, presented in Figs. 1-3. In these test simulations the total number of particles was not very large and equal to 16000. Figure 1 shows the evolution of the relative particle number error $\delta N/N$ for the normalized collisional frequencies $\nu^* = 0.018$ and $\nu^* = 0.035$ with the full collisional operator (3) (stars and circles) and only with the momentum correction term (8) (+ signs and squares).

Figure 2 shows the evolution of the relative energy error $\delta E/E$ for the normalized collisional frequencies $\nu^* = 0.018$ and $\nu^* = 0.035$ with the full collisional operator (3) (stars and circles) and only with the momentum correction term (8) (+ signs and squares). Applications with the full collisional operator (3) decrease the relative particle number error and the relative energy error by several orders of magnitude. This property provides more reliable and long steady-state results for the simulations with large number of collision times in agreement with the similar plots from Ref. [23]. Recently the successfull benchmark of the neoclassical transport, calculated by the FORTEC-3D code with the improved collisional operator (3) against global gyrokinetic particle-in-cell code ORB5 and theory has been reported in Ref. [25]. Good conservation properties of operator (3) have been also shown for the unlike-particle collisions in Ref. [26].

Figure 3 shows the evolution of the relative momen-

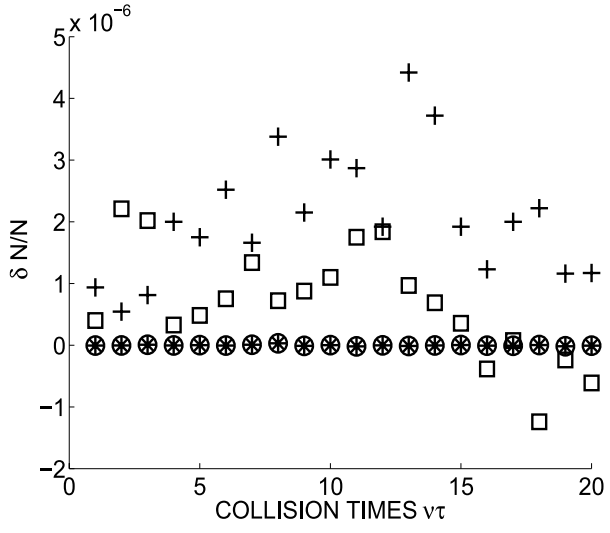

Fig. 1 Evolution of the relative particle number error ($\delta N/N$ versus collision times $\nu\tau$) is shown for the normalized collisional frequency $\nu^* = 0.035$ with the improved collisional operator (circles) and only with the momentum correction term (squares); for the normalized collisional frequency $\nu^* = 0.018$ with the improved collisional operator (stars) and only with the momentum correction term (crosses).

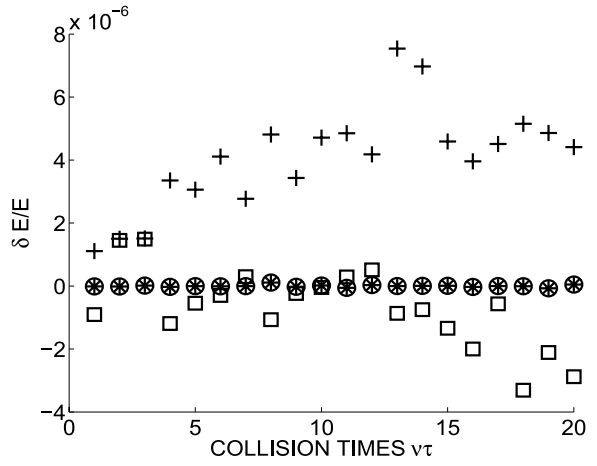

Fig. 2 Evolution of the relative energy error ($\delta E/E$ versus collision times $\nu\tau$) is shown for the normalized collisional frequency $\nu^* = 0.035$ with the improved collisional operator (circles) and only with the momentum correction term (squares); for the normalized collisional frequency $\nu^* = 0.018$ with the improved collisional operator (stars) and only with the momentum correction term (crosses).

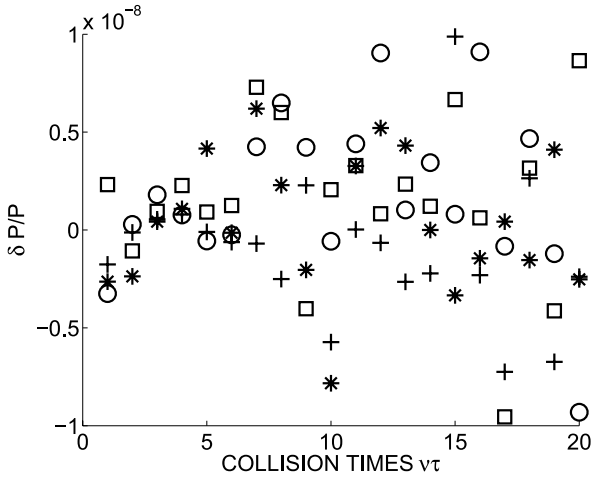

Fig. 3 Evolution of the relative momentum error ($\delta P/P$ versus collision times $\nu\tau$) is shown for the normalized collisional frequency $\nu^* = 0.035$ with the improved collisional operator (circles) and only with the momentum correction term (squares); for the normalized collisional frequency $\nu^* = 0.018$ with the improved collisional operator (stars) and only with the momentum correction term (crosses).

tum error $\delta P/P$ for the normalized collisional frequencies $\nu^* = 0.018$ and $\nu^* = 0.035$ with the full collisional operator (3) (stars and circles) and only with the momentum correction term (8) (+ signs and squares). This figure shows the near equivalence of Eqs. (3) and (8) with respect to the momentum correction; the modulus of the relative errors in both cases does not exceed the value of 10^{-8}.

The improved VENUS+δf collisional operator includes the additional energy scattering terms [13]. The corresponding terms, implemented into the DKES code, modify the bootstrap current of the Wendelstein-7X stellarator by 10-20% [27]. We present the effect of the energy scattering as well as the effect of the finite orbit width (FOW) with the VENUS+δf code for the LHD configurations in the next sections.

3. Bootstrap Current in the LHD Discharge #61863

Figure 4 shows the experimentally measured and smoothly fitted electron density (circles) and temperature (stars) profiles versus the normalized toroidal flux label s at $t = 3.1$ sec of the LHD discharge #61863 with $R_{\rm axis} = 3.90$ m. The electron density has a rather flat profile, while the temperature drops linearly. Motional Stark Effect measurements provide the rotational transform profile estimation and the corresponding total current of about 10 kA [20].

Additional details of these measurements, the experimental LHD setup, the determination of the bootstrap current and its uncertainties can be found in Refs. [3, 20]. In this discharge, balanced neutral beam injection has been used so the beam-induced current is small. The most probable candidate as a driving mechanism of the non-inductive current can be attributed to the bootstrap current.

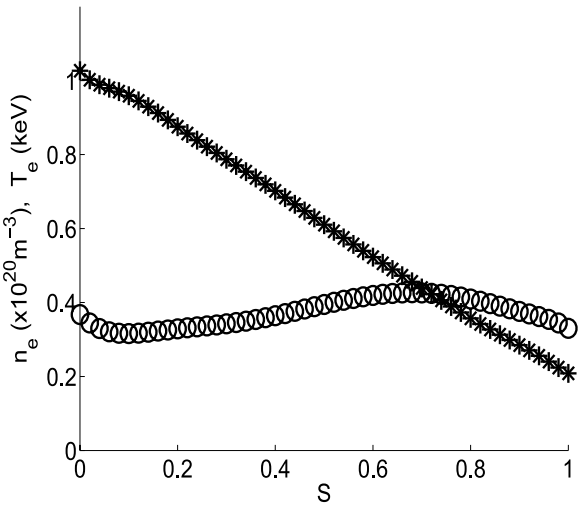

Fig. 4 The electron density (circles) and the temperature (stars) versus the flux label s for the LHD discharge #61863 ($R_{\rm axis} = 3.90$ m).

The bootstrap current flux derivatives $\mathrm{d}J_{\rm BS}/\mathrm{d}s$ as a function of the normalized flux s for the LHD discharge #61863 are presented in Fig. 5. The SPBSC and the TERPSICHORE code results in the collisionless limit are shown in Fig. 5 (a) as triangles and by the solid line, respectively. In the plasma core the SPBSC and the TERPSICHORE code results in the semi-analytical collisionless limit are almost the same. This means that the reconstruction to the Boozer coordinates, performed with the different magnetic field spectra width in these codes, leads to the same spatial dependencies. A difference is visible near the magnetic axis, where the numerically obtained equilibrium force balance is poor. Near the plasma edge, the TERPSICHORE code has found 2 resonant surfaces (2 spikes on the solid curve). In the collisionless regime (not ex-

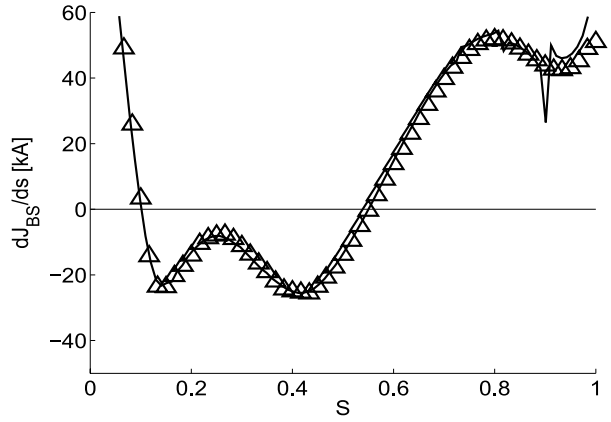

(a)

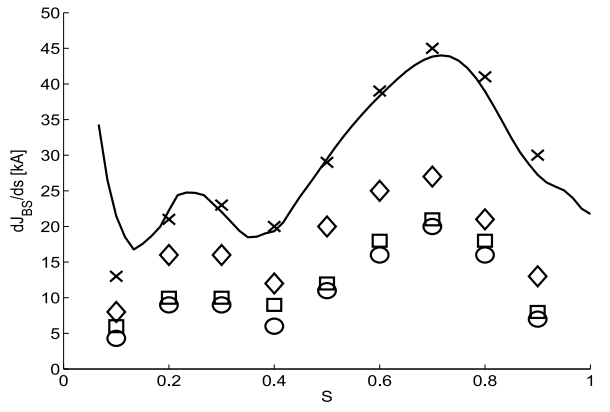

(b)

Fig. 5 (a): The LHD#61863 $R_{\rm axis} = 3.90$ m bootstrap current derivative $\mathrm{d}J_{\rm BS}/\mathrm{d}s$ versus the flux label s calculated in the collisionless limit with the SPBSC code (triangles), and with the TERPSICHORE code (solid line), (b): with the connection formula with the SPBSC code (solid line), with the VENUS+δf code (ii) method without the energy scattering, $A = 1$ (circles), with the energy scattering, $A = 1$ (squares) and $A =$ 2.e-3 (crosses), with (ei) method (diamonds).

perimentally relevant) the integration of the dJ_{BS}/ds function gives a total bootstrap current J_{BS} of 18 kA from the TERPSICHORE code in the Shaing-Callen limit and J_{BS} of 10 kA from the SPBSC code.

For the given experimental conditions the total bootstrap current of 27 kA is obtained from integration of the function dJ_{BS}/ds in the SPBSC code (Fig. 5 (b), solid line), using the connection formula between the collisionless and collisional limits.

In this paper with the usage of the VENUS+δf code we explore the effects of the finite orbit width on the bootstrap current for the LHD #61863 discharge. In the simulations we consider two different cases – protons with atomic mass $A = 1$ (wide orbits) and ions with artificial atomic mass $A =$ 2.e-3 (smaller orbit width). The average ratio of the orbit width with $A = 1$ to the temperature gradient length is on the level of 0.01.

The function dJ_{BS}/ds, calculated with the VENUS+δf code with (ii) method without the energy scattering and with atomic mass $A = 1$ is shown in Fig. 5 (b) by circles, the integration yields a total bootstrap current $J_{BS} =$ 10 kA. The functions dJ_{BS}/ds with the energy scattering are shown as squares for $A = 1.0$ (total bootstrap current is $J_{BS} = 12$ kA) and with crosses for $A =$ 2.e-3 (total bootstrap current is $J_{BS} = 26$ kA). The energy scattering effect increases the result by 10-20%. The function dJ_{BS}/ds, calculated with the VENUS+δf code with (ei) method, is shown in Fig. 5 (b) by diamonds and yields a total bootstrap current equal to 16 kA. The statistical results from the VENUS+δf code are obtained with 200000 markers with an accuracy 10% and do not depend on the integration time step size.

Under the given experimental conditions the electrons have thin orbits. However, heavy ions trapped in non-symmetric magnetic fields not subject to the orbit width limitation (or without the weight filter procedure) tend to accumulate their weights after a lengthy simulation time in regions far from their initial surface. This effect causes an impact on the bootstrap current that becomes excessively large. We have implemented in the VENUS+δf code the filter procedure to reinject the markers with very large weight δf (compare, for example, with variance reduction procedure in Ref. [28] or filtration in [19]). Figure 6 presents the typical influence of the filter size max $(\delta f/f)$, proportional to the spacial bin size Δs, on the function dJ_{BS}/ds at $s = 0.7$. One can see the significant "plateau" region, where the function dJ_{BS}/ds does not depend on value max $(\delta f/f)$ and reinjected particles do not change the result. We assume that the optimal filter size chosen should lie in this "plateau" region.

The total bootstrap current J_{BS} of 10-12 kA obtained with the ions for $A = 1$, calculated with the VENUS+δf code, is in good agreement with the experimentally obtained total bootstrap current of 10 kA. Smaller orbit width for the ions with atomic mass $A =$ 2.e-3 from the VENUS+δf code yields the total bootstrap current of

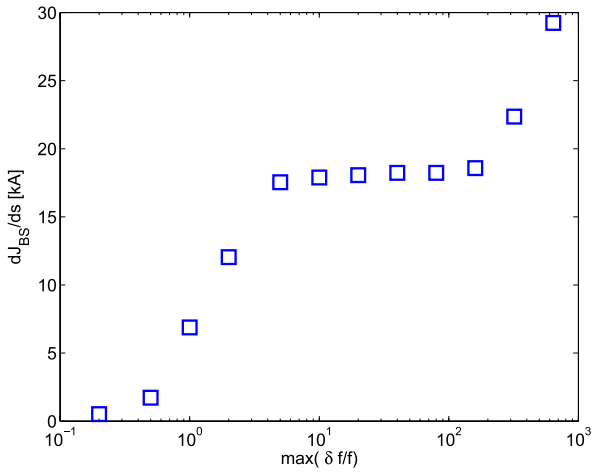

Fig. 6 Particle weight filter max $(\delta f/f)$ study for ions with $A = 1$, performed for the LHD#61863 $R_{axis} = 3.90$ m bootstrap current derivative dJ_{BS}/ds on $s = 0.7$ with the VENUS+δf code.

Table 1 The LHD#61863 total bootstrap current from the experimental observation (column #1), from the SPBSC code with the connection formula (column #2) and in the collisionless limit (column #3), from the TERPSICHORE code (column #4), from the VENUS+δf code without the energy scattering, $A = 1$ (column #5), with the energy scattering, $A = 1$ (column #6) and $A =$ 2.e-3 (column #7), with (ei) method (column #8).

	1	2	3	4	5	6	7	8
J_{BS} (kA)	10	27	10	18	10	12	26	16

$J_{BS} = 26$ kA, (ei) method also with small orbit width yields $J_{BS} = 16$ kA. The summary of this section is shown in Table 1.

4. Bootstrap Current in the LHD Discharge #82582

Figure 7 shows the experimentally measured and smoothly fitted electron density (circles) and temperature (stars) profiles versus the normalized toroidal flux label s at $t = 3.9$ sec of the LHD discharge #82582 with $R_{axis} =$ 4.05 m.

The bootstrap current derivatives dJ_{BS}/ds in the collisionless limit for the LHD discharge #82582 as a function of the normalized flux s are presented in Fig. 8 (a) with triangles (calculated with the SPBSC code) and with the solid line (from the TERPSICHORE code). The bootstrap current derivative calculated with the TERPSICHORE code, has several visible resonant spikes. The integration of the dJ_{BS}/ds function, obtained in the collisionless limit with the SPBSC and the TERPSICHORE codes, yields small negative total bootstrap currents J_{BS} of about -2 kA.

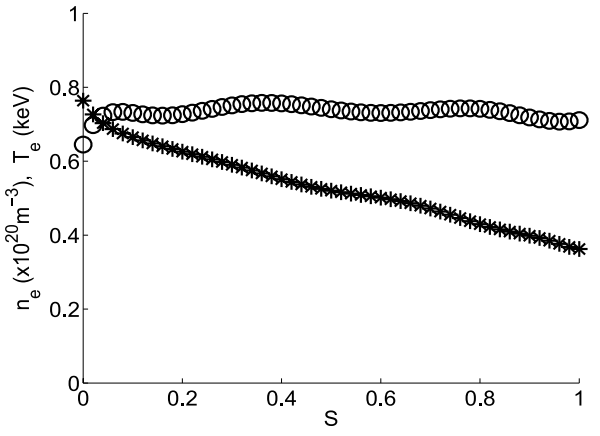

Fig. 7 The electron density (circles) and the temperature (stars) versus the flux label s for the LHD discharge #82582 ($R_{\rm axis}$ = 4.05 m).

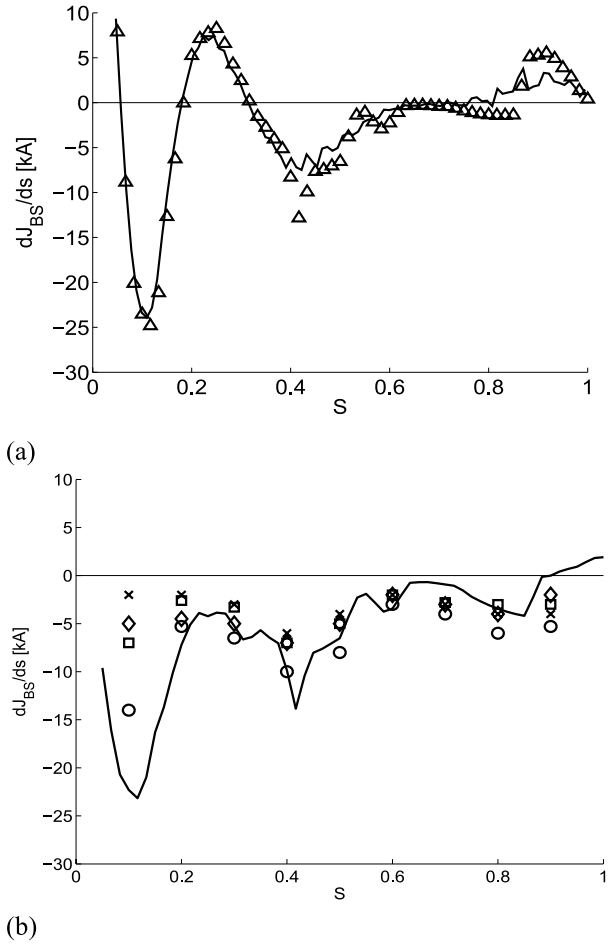

Fig. 8 (a): The LHD#82582 $R_{\rm axis}$ = 4.05 m bootstrap current derivative $\mathrm{d}J_{\rm BC}/\mathrm{d}s$ versus the flux label s calculated in the collisionless limit with the SPBSC code (triangles) and with the TERPSICHORE code (solid line), (b): with the connection formula with the SPBSC code (solid line), with the VENUS+δf code with (ii) method without energy scattering A = 1.e-3 (circles), with energy scattering A = 1.e-3 (squares), A = 1 (crosses), with (ei) method (diamonds).

The bootstrap current derivative $\mathrm{d}J_{\rm BS}/\mathrm{d}s$ for the LHD discharge #82582 from the connection formula in the SBPSC code is presented in Fig. 8 (b) with the solid line. The total bootstrap current from this code is $J_{\rm BS}$ = −5.5 kA. VENUS+δf code results with atomic mass A = 1.e-3 (small orbit width) without the energy scattering are shown with circles, with energy scattering, these are shown as squares for A = 1.e-3 and as crosses for A = 1.0 (finite orbit width effect). VENUS+δf code results with (ei) method are shown with diamonds.

The total bootstrap current, calculated with the VENUS+δf code is equal to −6.2 kA without the energy scattering and equal to −3.5 kA with energy scattering for the ions with the artificial atomic mass A = 1.e-3, which is close to $J_{\rm BS}$ = −3.8 kA from (ei) method. The energy scattering effect is more visible for the LHD discharge #82582 than for the LHD discharge #61863 according to the VENUS+δf code simulations.

Finite orbit width for the ions with A = 1 and with the energy scattering yields small negative total bootstrap current of −3.0 kA. The absolute value of experimentally measured total current of −14 kA is larger than the bootstrap currents obtained from the SBPSC and VENUS+δf codes (see Table 2 as a summary of this section).

Table 2 The LHD#82582 total bootstrap current (kA) from the experimental observation (column #1), from the SPBSC code with the connection formula (column #2) and in the collisionless limit (column #3), from the TERPSICHORE code (column #4), from the VENUS+δf code with (ii) method without the energy scattering, A = 1.e-3 (column #5), with the energy scattering, A = 1.e-3 (column #6) and A = 1 (column #7), with (ei) method (column #8).

	1	2	3	4	5	6	7	8
$J_{\rm BS}$	−14	−5.5	−2.0	−2.0	−6.2	−3.5	−3.0	−3.8

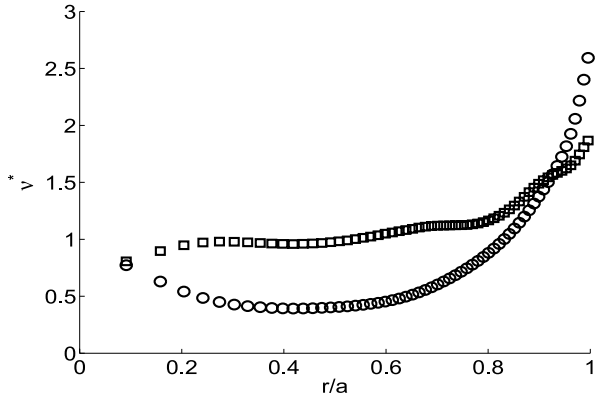

Fig. 9 The normalized collisional frequency ν^* versus the normalized plasma radius $r/a = s^{0.5}$, calculated with the SPBSC code, corresponding to the LHD discharges #61863 (circles) and #82582 (squares).

Figure 9 shows the normalized collisional frequency ν^* profiles, calculated with the SPBSC code, corresponding to the LHD discharges #61863 (circles) and #82582 (squares). For these discharges, the normalized collisional frequency is enclosed in the interval [0.5 – 2.5] and belongs to plateau collisional regime.

5. Summary and Discussion

Bootstrap current simulations for the experimental Heliotron LHD discharges #61863 and #82582 have been performed with the 3D neoclassical codes SPBSC, TERPSICHORE (only as a test in the collisionless limit) and with the VENUS+δf code with the improved conservative operator. This work constitutes a further step towards increasing the accuracy of the 3D simulation tools and the applications of the exact input experimental data (electron temperature and density, complicated shape of the boundary magnetic surface). However, taking into account the significant role of the turbulent transport in plasmas, it is not clear at this time how accurate and how close to the experimental results could our numerical tools, based only on neoclassical approaches, be.

Different bootstrap current models, implemented into the 3D neoclassical codes SPBSC and VENUS+δf, show an agreement with the experimentally obtained positive total bootstrap current of 10 kA in the LHD discharge #61863 with the magnetic axis of $R_{\rm axis} = 3.90$ m and negative total bootstrap current of -14 kA in the LHD discharge #82582 with $R_{\rm axis} = 4.05$ m. The difference of the current profiles between the SPBSC connection formula prediction and the VENUS+δf code simulation can be also partially explained by the difference between the experimentally obtained rotational transform profiles with the error bars [19] and the corresponding time-dependent rotational transform based on the SPBSC simulation.

Energy scattering effects implemented into the VENUS+δf code change the total bootstrap current by 10-20% for the LHD discharge #61863. For the LHD discharge #82582 the energy scattering effect with the VENUS+δf code changes the bootstrap current by a factor of 2, however, the total bootstrap current for this case is rather small. Finite orbit widths with the VENUS+δf code due to the different marker masses can significantly change the absolute value of the simulated ion bootstrap current for both LHD #61863 and LHD#82582 discharges.

Accurate bootstrap current simulations include the electric field and inductive current effects as well as the non-equal impact of electrons and ions as it was recently done with the DKES, NEO-MC and MOCA codes for the TJ-II stellarator [29, 30]. In our paper we have also made the additional simulations with the ambipolar radial electric field simulation (ion root) and with the different impact of electrons and ions - with (ei) method. The difference between the total bootstrap current, computed with (ii) method and with (ei) method for these given LHD discharges, has been presented in our paper.

Acknowledgments

The work was supported in part by the NIFS/NINS under the project of International Network of Scientific Collaboration (Japan), by the budget NIFS11ULPP022, by CRPP (Switzerland), by the Fonds National Suisse de la Recherché Scientifique, by Euratom, by the RosAtom Contract H.4A.52.90.12.1006, by grant 4361.2012.2 of President of Russian Federation for Leading Scientific Schools. The computational results were performed on clusters CSCS, Pleiades2 (Switzerland), Opteron (NIFS, Japan), LSPP-ITER (Kurchatov Institute, Russia). M. Isaev thanks C.D. Beidler and H. Maaβberg (IPP, Greifswald) for their valuable comments and corrections.

[1] K.Y. Watanabe *et al*., Nucl. Fusion **35**, 335 (1995).
[2] K. Shaing and J. Callen, Phys. Fluids **26**, 3315 (1983).
[3] K.Y. Watanabe *et al*., J. Plasma Fusion Res. SERIES **5**, 124 (2002).
[4] W.A. Cooper *et al*., Plasma Phys. Control. Fusion **44**, 1 (2002).
[5] D.V. Anderson *et al*., J. Supercomput. Appl. **4**, 34 (1990).
[6] A.H. Boozer, Phys. Fluids **24**, 1999 (1981).
[7] M. Murakami *et al*., Phys. Rev. Lett. **66**, 707 (1991).
[8] H. Maaβberg *et al*., Plasma Phys. Control. Fusion **47**, 1137 (2005).
[9] W.I. Van Rij and S.P. Hirshman, Phys. Fluids B **1**, 563 (1989).
[10] C.D. Beidler *et al*., Proc. 30th EPS Conf. on Control. Fusion and Plasma Phys. (St. Petersburg, Russia 2003) ECA **27**A, P3.2 (2003).
[11] Y. Ogawa *et al*., Nucl. Fusion **32**, 119 (1992).
[12] M.Yu. Isaev *et al*., Fusion Sci. Technol. **50**, 440 (2006).
[13] A.H. Boozer and G. Kuo-Petravic, Phys. Fluids **24**, 851 (1981).
[14] C.D. Beidler *et al*., Proc. 22nd IAEA Fusion Energy Conf., Geneva, Switzerland, TH/P8-10 (2008).
[15] K. Allmaier *et al*., CDROM with Proc. of Joint Conf. of 17th Int. Toki Conf. on Physics of Flow and Turbulence in Plasmas and 16th Int. Stellarator/Heliotron Workshop, 615 (2007).
[16] C.D. Beidler *et al*., Nucl. Fusion **51**, 076001 (2011).
[17] M.Yu. Isaev *et al*., Plasma Fusion Res. **3**, 036 (2008).
[18] M.Yu. Isaev *et al*., Nucl. Fusion **49**, 075013 (2009).
[19] S. Satake *et al*., Plasma Fusion Res. **3**, S1062 (2008).
[20] Y. Nakamura *et al*., Proc. 22nd IAEA Fusion Energy Conf Geneva Switzerland EX/P6-20 (2008).
[21] O. Fischer *et al*., Nucl. Fusion **42**, 817 (2002).
[22] R. Sanchez *et al*., Comput. Phys. Commun. **141**, 55 (2001).
[23] W.X. Wang *et al*., Plasma Phys. Control. Fusion **41**, 1091 (1999).
[24] A. Bergmann *et al*., Phys. Plasmas **8**, 5192 (2001).
[25] T. Vernay *et al*., Phys. Plasmas **17**, 122301 (2010).
[26] R.A. Kolesnikov *et al*., J. Comput. Phys. **229**, 5564 (2010).
[27] H. Maaβberg and C.D. Beidler, Phys. Plasmas **17**, 052507 (2010).
[28] K. Allmaier *et al*., Phys. Plasmas **15**, 072512 (2008).
[29] J.L. Velasco *et al*., Plasma Phys. Control. Fusion **53**, 115014 (2011).
[30] V. Tribaldos *et al*., Phys. Plasmas **18**, 102507 (2011).